Greens functions - solution for earth's surface movement due to a slipping patch at depth

Need to know slip distribution along the fault as a function of time

$$u_n(\mathbf{x}, t) = \int_{-\infty}^{\infty} d\tau \iint_{\Sigma} [u_i(\boldsymbol{\xi}, \tau)] c_{ijpq} \nu_j \frac{\partial G_{np}(\mathbf{x}, t-\tau; \boldsymbol{\xi}, 0)}{\partial \xi_q} d\Sigma$$

$$c_{ijpq} = \lambda \delta_{ij} \delta_{kl} + \mu(\delta_{ik}\delta_{jl} + \delta_{il}\delta_{jk}),$$

No closed-form solution for Greens functions (G_{np}). Makes use of full-space solution and image solution (recall Segall's 2D dislocation static solutions)

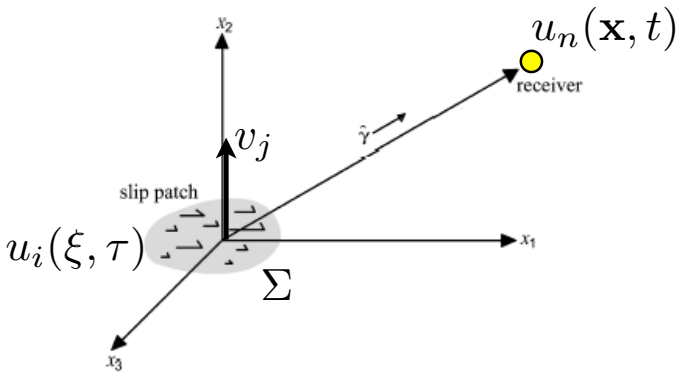

Greens functions: displacements due to unit slip on a fault "patch"

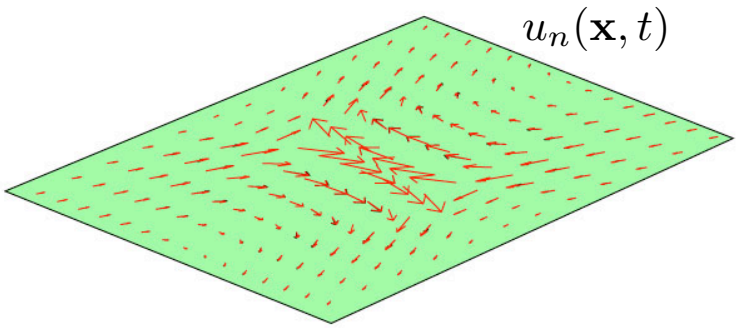

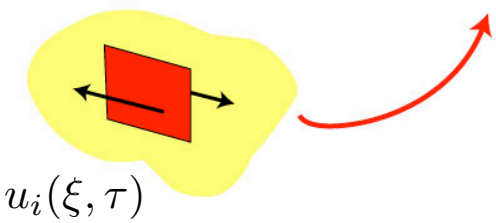

Analytical solutions for shear dislocation in an elastic halfspace
Okada, 1985

$$u_n(\mathbf{x}, t) = \int_{-\infty}^{\infty} d\tau \iint_{\Sigma} [u_i(\boldsymbol{\xi}, \tau)] c_{ijpq} \nu_j \frac{\partial G_{np}(\mathbf{x}, t-\tau; \boldsymbol{\xi}, 0)}{\partial \xi_q} d\Sigma$$

Full-space solution: displacement at a point due to a dislocation

$$\mathbf{u}(\mathbf{x},t) = \frac{1}{4\pi\rho}\mathbf{A}^N\frac{1}{r^4}\int_{r/\alpha}^{r/\beta}\tau M_0(t-\tau)\,d\tau + \frac{1}{4\pi\rho\alpha^2}\mathbf{A}^{IP}\frac{1}{r^2}M_0\left(t-\frac{r}{\alpha}\right) + \frac{1}{4\pi\rho\beta^2}\mathbf{A}^{IS}\frac{1}{r^2}M_0\left(t-\frac{r}{\beta}\right) + \frac{1}{4\pi\rho\alpha^3}\mathbf{A}^{FP}\frac{1}{r}\dot{M}_0\left(t-\frac{r}{\alpha}\right) + \frac{1}{4\pi\rho\beta^3}\mathbf{A}^{FS}\frac{1}{r}\dot{M}_0\left(t-\frac{r}{\beta}\right), \quad (8)$$

where the radiation pattern terms are

$$\mathbf{A}^N = 9\sin 2\theta\cos\varphi\hat{\mathbf{r}} - 6(\cos 2\theta\cos\varphi\hat{\boldsymbol{\theta}} - \cos\theta\sin\varphi\hat{\boldsymbol{\varphi}})$$
$$\mathbf{A}^{IP} = 4\sin 2\theta\cos\varphi\hat{\mathbf{r}} - 2(\cos 2\theta\cos\varphi\hat{\boldsymbol{\theta}} - \cos\theta\sin\varphi\hat{\boldsymbol{\varphi}})$$
$$\mathbf{A}^{IS} = -3\sin 2\theta\cos\varphi\hat{\mathbf{r}} + 3(\cos 2\theta\cos\varphi\hat{\boldsymbol{\theta}} - \cos\theta\sin\varphi\hat{\boldsymbol{\varphi}})$$
$$\mathbf{A}^{FP} = \sin 2\theta\cos\varphi\hat{\mathbf{r}}$$
$$\mathbf{A}^{FS} = (\cos 2\theta\cos\varphi\hat{\boldsymbol{\theta}} - \cos\theta\sin\varphi\hat{\boldsymbol{\varphi}}). \quad (9)$$

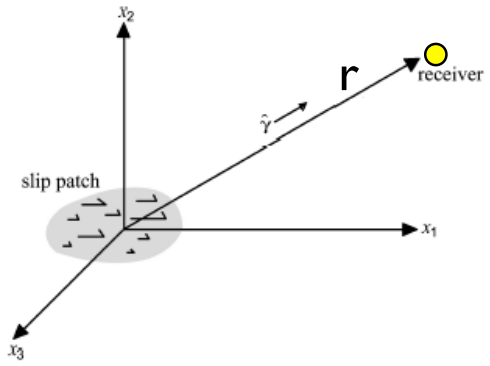

FIGURE 4 A coordinate system for analysis of far-field radiation at receiver with distance r_0 and angle $\hat{\gamma}$ from a fault with unidirectional slip $\Delta u = [\Delta u_1(x_1, x_3, t), 0, 0]$.

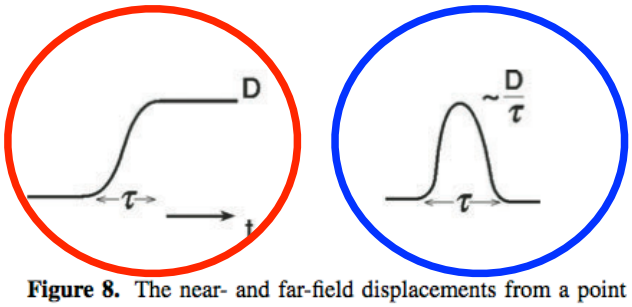

Figure 8. The near- and far-field displacements from a point dislocation seismic source which represents a fault slip motion given by a ramp function with duration τ.

near- and intermediate field terms

far-field terms (P and S wave)

$$\mathbf{u}(\mathbf{x},t) = \frac{1}{4\pi\rho}\mathbf{A}^N\frac{1}{r^4}\int_{r/\alpha}^{r/\beta}\tau M_0(t-\tau)\,d\tau + \frac{1}{4\pi\rho\alpha^2}\mathbf{A}^{IP}\frac{1}{r^2}M_0\left(t-\frac{r}{\alpha}\right) + \frac{1}{4\pi\rho\beta^2}\mathbf{A}^{IS}\frac{1}{r^2}M_0\left(t-\frac{r}{\beta}\right) + \frac{1}{4\pi\rho\alpha^3}\mathbf{A}^{FP}\frac{1}{r}\dot{M}_0\left(t-\frac{r}{\alpha}\right) + \frac{1}{4\pi\rho\beta^3}\mathbf{A}^{FS}\frac{1}{r}\dot{M}_0\left(t-\frac{r}{\beta}\right), \quad (8)$$

where the radiation pattern terms are

$$\mathbf{A}^N = 9\sin 2\theta\cos\varphi\hat{\mathbf{r}} - 6(\cos 2\theta\cos\varphi\hat{\boldsymbol{\theta}} - \cos\theta\sin\varphi\hat{\boldsymbol{\varphi}})$$
$$\mathbf{A}^{IP} = 4\sin 2\theta\cos\varphi\hat{\mathbf{r}} - 2(\cos 2\theta\cos\varphi\hat{\boldsymbol{\theta}} - \cos\theta\sin\varphi\hat{\boldsymbol{\varphi}})$$
$$\mathbf{A}^{IS} = -3\sin 2\theta\cos\varphi\hat{\mathbf{r}} + 3(\cos 2\theta\cos\varphi\hat{\boldsymbol{\theta}} - \cos\theta\sin\varphi\hat{\boldsymbol{\varphi}})$$
$$\mathbf{A}^{FP} = \sin 2\theta\cos\varphi\hat{\mathbf{r}}$$
$$\mathbf{A}^{FS} = (\cos 2\theta\cos\varphi\hat{\boldsymbol{\theta}} - \cos\theta\sin\varphi\hat{\boldsymbol{\varphi}}). \quad (9)$$

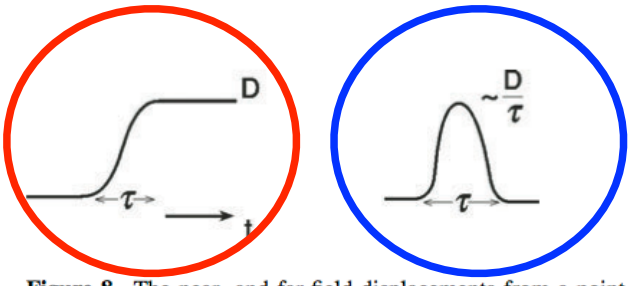

Figure 8. The near- and far-field displacements from a point dislocation seismic source which represents a fault slip motion given by a ramp function with duration τ.

$$\mathbf{u}(\mathbf{x},t) = \frac{1}{4\pi\rho}\mathbf{A}^N\frac{1}{r^4}\int_{r/\alpha}^{r/\beta}\tau M_0(t-\tau)\,d\tau + \frac{1}{4\pi\rho\alpha^2}\mathbf{A}^{IP}\frac{1}{r^2}M_0\left(t-\frac{r}{\alpha}\right) + \frac{1}{4\pi\rho\beta^2}\mathbf{A}^{IS}\frac{1}{r^2}M_0\left(t-\frac{r}{\beta}\right) + \frac{1}{4\pi\rho\alpha^3}\mathbf{A}^{FP}\frac{1}{r}\dot{M}_0\left(t-\frac{r}{\alpha}\right) + \frac{1}{4\pi\rho\beta^3}\mathbf{A}^{FS}\frac{1}{r}\dot{M}_0\left(t-\frac{r}{\beta}\right), \quad (8)$$

where the radiation pattern terms are

$$\begin{aligned}
\mathbf{A}^N &= 9\sin 2\theta\cos\varphi\hat{\mathbf{r}} - 6(\cos 2\theta\cos\varphi\hat{\boldsymbol{\theta}} - \cos\theta\sin\varphi\hat{\boldsymbol{\varphi}})\\
\mathbf{A}^{IP} &= 4\sin 2\theta\cos\varphi\hat{\mathbf{r}} - 2(\cos 2\theta\cos\varphi\hat{\boldsymbol{\theta}} - \cos\theta\sin\varphi\hat{\boldsymbol{\varphi}})\\
\mathbf{A}^{IS} &= -3\sin 2\theta\cos\varphi\hat{\mathbf{r}} + 3(\cos 2\theta\cos\varphi\hat{\boldsymbol{\theta}} - \cos\theta\sin\varphi\hat{\boldsymbol{\varphi}})\\
\mathbf{A}^{FP} &= \sin 2\theta\cos\varphi\hat{\mathbf{r}}\\
\mathbf{A}^{FS} &= (\cos 2\theta\cos\varphi\hat{\boldsymbol{\theta}} - \cos\theta\sin\varphi\hat{\boldsymbol{\varphi}}).
\end{aligned} \quad (9)$$

near- and intermediate field terms

"near field" and "intermediate field" displacement is proportional to moment.

It results in permanent ground displacement.

Drops off as $1/r^4$ and $1/r^2$.

far-field terms (P and S wave)

"far field" displacement is proportional to moment rate, not moment.

It goes to 0 because moment rate goes to 0.

"far field" displacement decreases as $1/r$

"far field" equations apply if

$$\lambda >> \frac{2L^2}{r}$$

dislocation patch is normal to the plotted plane

ϕ is 0 in the plotted plane

$$\mathbf{u}(\mathbf{x},t) = \frac{1}{4\pi\rho}\mathbf{A}^N\frac{1}{r^4}\int_{r/\alpha}^{r/\beta}\tau M_0(t-\tau)\,d\tau + \frac{1}{4\pi\rho\alpha^2}\mathbf{A}^{IP}\frac{1}{r^2}M_0\left(t-\frac{r}{\alpha}\right) + \frac{1}{4\pi\rho\beta^2}\mathbf{A}^{IS}\frac{1}{r^2}M_0\left(t-\frac{r}{\beta}\right) + \frac{1}{4\pi\rho\alpha^3}\mathbf{A}^{FP}\frac{1}{r}\dot{M}_0\left(t-\frac{r}{\alpha}\right) + \frac{1}{4\pi\rho\beta^3}\mathbf{A}^{FS}\frac{1}{r}\dot{M}_0\left(t-\frac{r}{\beta}\right), \quad (8)$$

where the radiation pattern terms are

$$\begin{aligned}
\mathbf{A}^N &= 9\sin 2\theta\cos\varphi\hat{\mathbf{r}} - 6(\cos 2\theta\cos\varphi\hat{\boldsymbol{\theta}} - \cos\theta\sin\varphi\hat{\boldsymbol{\varphi}})\\
\mathbf{A}^{IP} &= 4\sin 2\theta\cos\varphi\hat{\mathbf{r}} - 2(\cos 2\theta\cos\varphi\hat{\boldsymbol{\theta}} - \cos\theta\sin\varphi\hat{\boldsymbol{\varphi}})\\
\mathbf{A}^{IS} &= -3\sin 2\theta\cos\varphi\hat{\mathbf{r}} + 3(\cos 2\theta\cos\varphi\hat{\boldsymbol{\theta}} - \cos\theta\sin\varphi\hat{\boldsymbol{\varphi}})\\
\mathbf{A}^{FP} &= \sin 2\theta\cos\varphi\hat{\mathbf{r}}\\
\mathbf{A}^{FS} &= (\cos 2\theta\cos\varphi\hat{\boldsymbol{\theta}} - \cos\theta\sin\varphi\hat{\boldsymbol{\varphi}}).
\end{aligned} \quad (9)$$

P wave

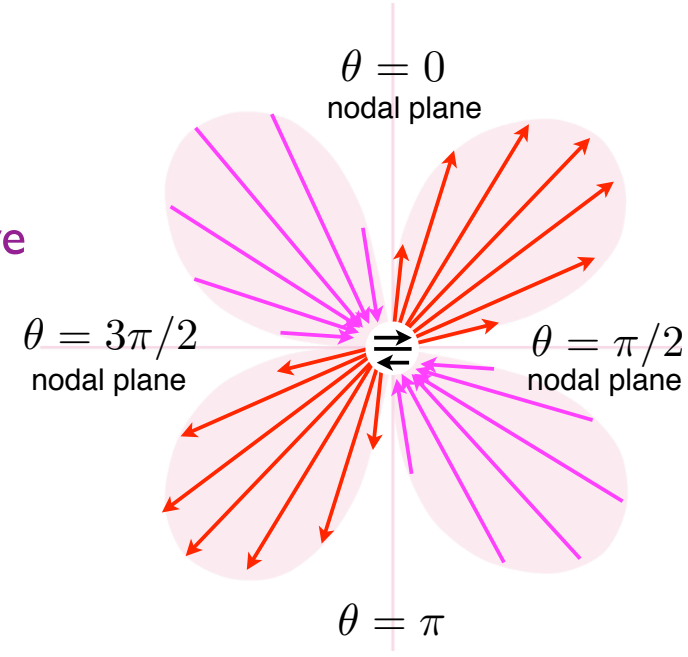

dislocation patch is
normal to the plotted plane

ϕ is 0 in the plotted plane

$$\mathbf{u}(\mathbf{x}, t) = \frac{1}{4\pi\rho}\mathbf{A}^N \frac{1}{r^4}\int_{r/\alpha}^{r/\beta} \tau M_0(t-\tau)\,d\tau + \frac{1}{4\pi\rho\alpha^2}\mathbf{A}^{IP}\frac{1}{r^2}M_0\left(t-\frac{r}{\alpha}\right) + \frac{1}{4\pi\rho\beta^2}\mathbf{A}^{IS}\frac{1}{r^2}M_0\left(t-\frac{r}{\beta}\right) + \frac{1}{4\pi\rho\alpha^3}\mathbf{A}^{FP}\frac{1}{r}\dot{M}_0\left(t-\frac{r}{\alpha}\right) + \frac{1}{4\pi\rho\beta^3}\mathbf{A}^{FS}\frac{1}{r}\dot{M}_0\left(t-\frac{r}{\beta}\right), \quad (8)$$

S wave

where the radiation pattern terms are

$$\mathbf{A}^N = 9\sin 2\theta\cos\varphi\hat{\mathbf{r}} - 6(\cos 2\theta\cos\varphi\hat{\boldsymbol{\theta}} - \cos\theta\sin\varphi\hat{\boldsymbol{\varphi}})$$
$$\mathbf{A}^{IP} = 4\sin 2\theta\cos\varphi\hat{\mathbf{r}} - 2(\cos 2\theta\cos\varphi\hat{\boldsymbol{\theta}} - \cos\theta\sin\varphi\hat{\boldsymbol{\varphi}})$$
$$\mathbf{A}^{IS} = -3\sin 2\theta\cos\varphi\hat{\mathbf{r}} + 3(\cos 2\theta\cos\varphi\hat{\boldsymbol{\theta}} - \cos\theta\sin\varphi\hat{\boldsymbol{\varphi}})$$
$$\mathbf{A}^{FP} = \sin 2\theta\cos\varphi\hat{\mathbf{r}}$$
$$\mathbf{A}^{FS} = (\cos 2\theta\cos\varphi\hat{\boldsymbol{\theta}} - \cos\theta\sin\varphi\hat{\boldsymbol{\varphi}}). \quad (9)$$

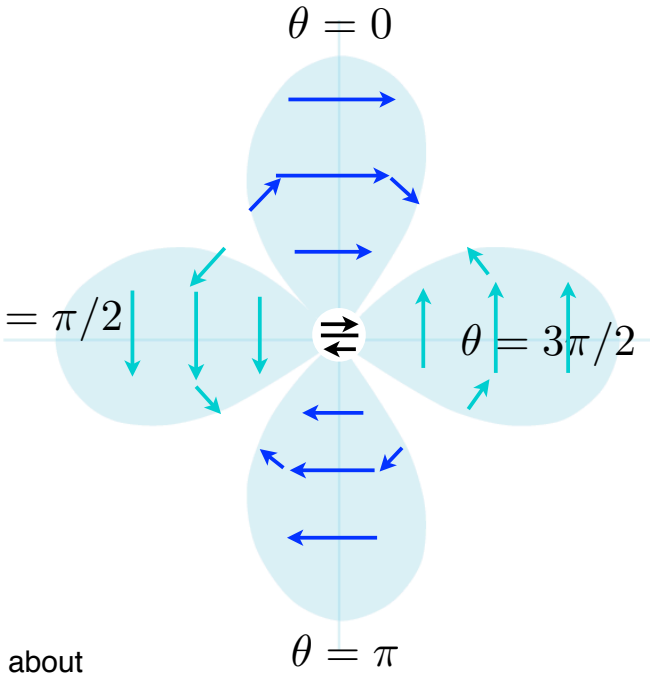

$\alpha = \sqrt{3}\beta$ so the S wave amplitude is about 5 times bigger than the P wave

p 945 - amplitude of the Fourier transform of a "one-sided pulse" at very low frequencies equals the area under the pulse (e.g. EQ 11). Thus it's proportional to moment.

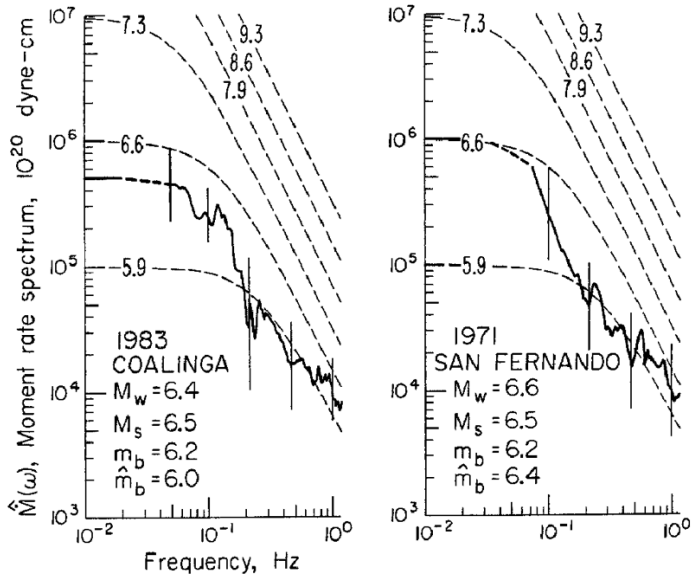

FIG. 8. Moment rate spectra for two California earthquakes. See legend to Figure 7.

p 945 -also, corner frequency is inversely proportional to the duration of the pulse, so dimension of the source can be obtained (Brune EQ from last time): $r = \dfrac{2.34\beta}{2\pi f_c}$

	Circular ($\lambda = \mu$)	Strike Slip	Dip Slip
Stress drop ($\Delta\sigma$)	$\frac{7\pi}{16}\mu\frac{(\bar{D})}{a}$	$\frac{2}{\pi}\mu\left(\frac{\bar{D}}{w}\right)$	$\frac{4(\lambda+\mu)}{\pi(\lambda+2\mu)}\mu\left(\frac{\bar{D}}{w}\right)$
Strain energy ($\Delta W = S\sigma D$)	$\frac{16}{7\mu}a^3\Delta\sigma\bar{\sigma}$	$\frac{\pi}{2\mu}w^2L\Delta\sigma\bar{\sigma}$	$\frac{\pi(\lambda+2\mu)}{4(\lambda+\mu)\mu}w^2L\Delta\sigma\bar{\sigma}$
Moment ($M_o = \mu S\bar{D}$)	$\frac{16}{7}\Delta\sigma a^3$	$\frac{\pi}{2}\Delta\sigma w^2L$	$\frac{\pi(\lambda+2\mu)}{4(\lambda+\mu)}\Delta\sigma w^2L$

FIG. 1. Relations between stress drop, strain energy, offset, dimension, and moment for static cracks. Dimensions of the fault are a radius, L length, w width; initial stress is σ_0; final stress is σ_1; stress drop is $\Delta\sigma = \sigma_0 - \sigma_1$; average stress is $\bar{\sigma} = (\sigma_0+\sigma_1)/2$; average dislocation is $\bar{D}$.

$$\Delta\sigma = \frac{7}{16}\frac{M_o}{r^3}$$

Finite source models - page 947

needed when observer is close to fault and for permanent displacement (near field), and to understand directivity effect (near and far field)

Brune (1970) self-similar crack: as slip grows, crack dimension grows.
Haskell (1964) slip on a rectangular fault idealized as a propagating ramp (carpet wrinkle analogy)
Duration of slip is far shorter than duration of the quake
Demonstrated by Tom Heaton, 1990.

Kinematic vs. dynamic rupture models

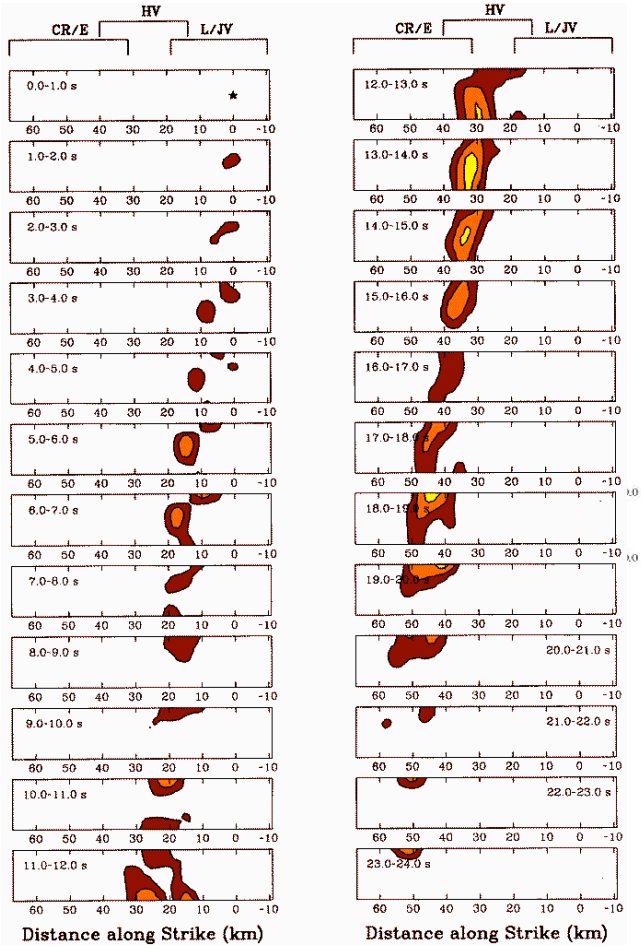

This looks sort of like the Haskell propagating ramp.

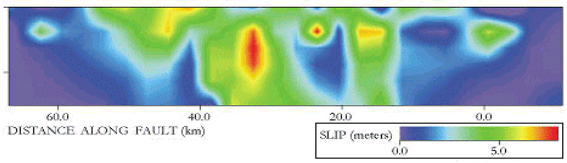

Wald and Heaton, 1994

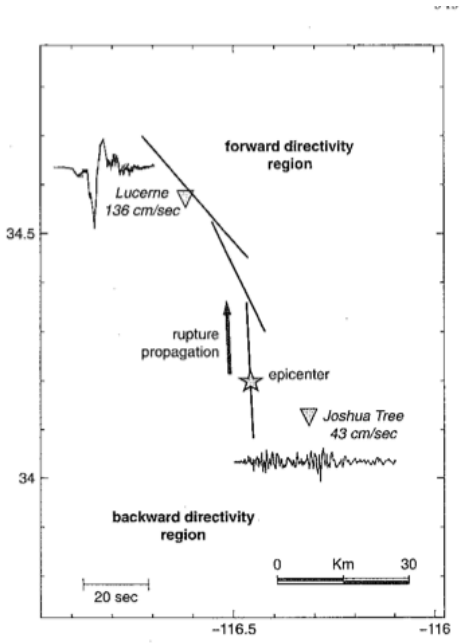

FIGURE 13 Illustration of directivity in velocity pulses recorded in the 1992 Landers, California, earthquake. Rupture propagated north from the epicenter, away from the station at Joshua Tree (with the long, low-amplitude velocity trace) and toward the Lucerne station (with the stronger, compact velocity pulse). From Somerville *et al.*, 1997.

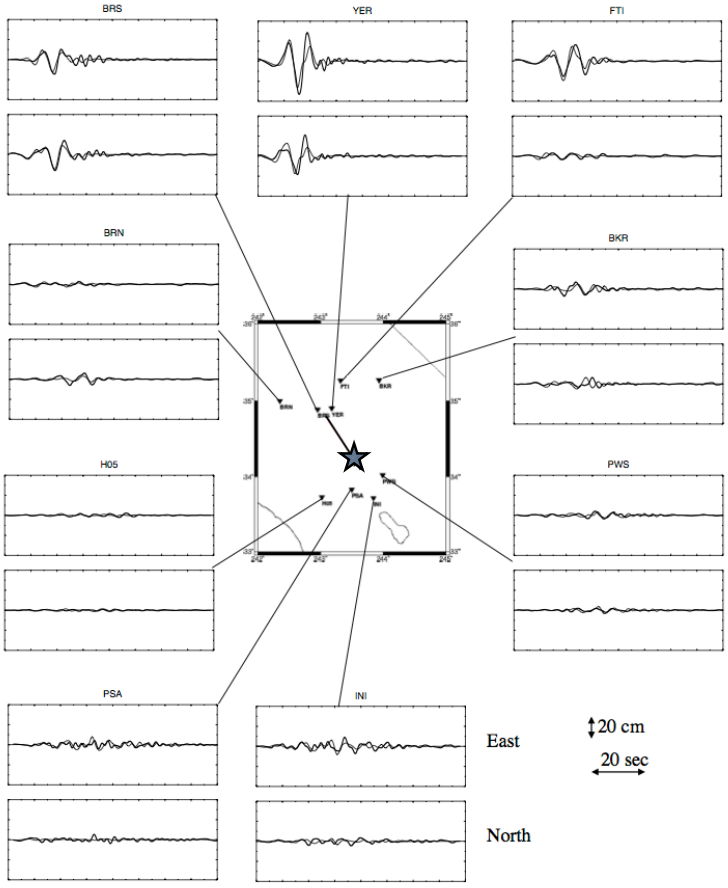

Directivity effects

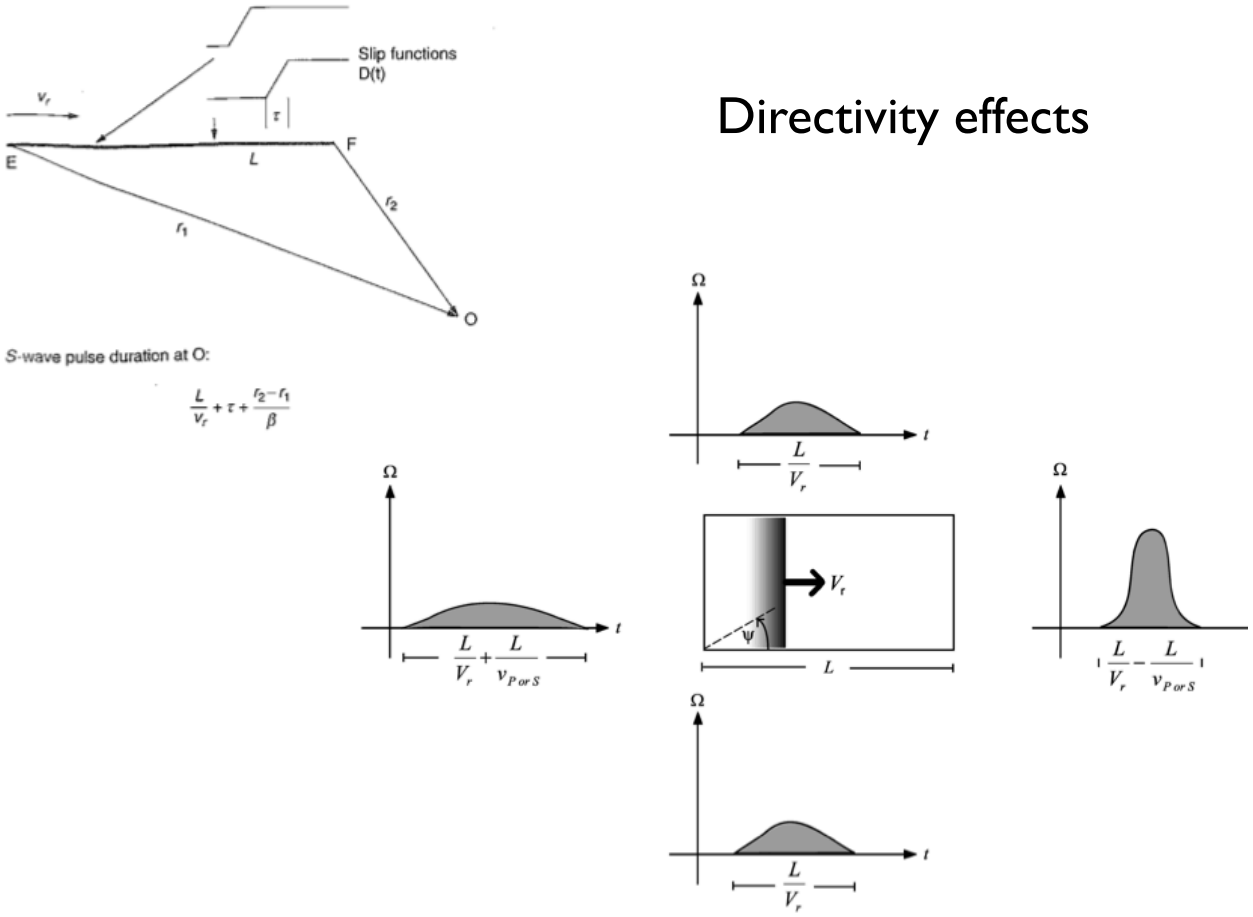

Propagation effects (on strong motion)

scattering and attenuation

loss of high frequencies ("f_{max}")
loss goes as $exp^{-\pi\kappa f}$
κ is bigger in sed basins (fig. 16)

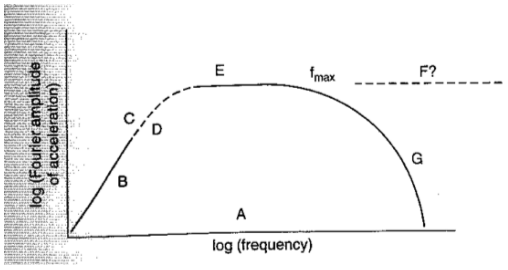

sedimentary basins

larger amplitudes, longer duration,
surface waves generated at edge of basin (strong, late arrivals)
<u>focusing</u> of seismic energy (Kobe; Northridge/Santa Monica)

nonlinear elasticity near the surface

soft sediments in top few hundred m amplify shaking
because wave propagation is slowed down - **nonlinearity** decreases seis veloc
at high diff stress, making lower frequencies resonate, + damping shaking more.

Propagation effects (on strong motion)

sedimentary basins

larger amplitudes, longer duration,
also - high frequencies are lost to attenuation
example from sites on rock and in sed basin: 1985 Mexico City earthquake

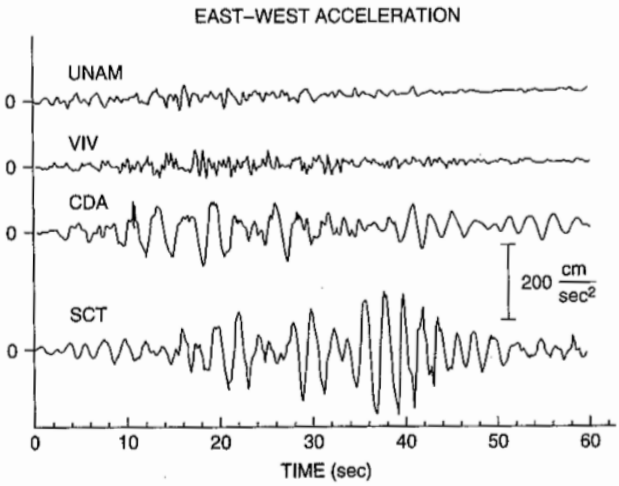

FIGURE 17 Most significant one-minute segment of strong-motion accelerograms recorded at four stations in Mexico City, in the September 19, 1985, earthquake ($M = 8.0$). Stations are 350 km from the epicenter, so differences can only be attributed to differences in geological conditions at the site. No time correlation exists among these traces (from Anderson *et al.*, 1986).

Topographic Effects

topography: topo wavelength close to S wave wavelength leads to amplification of shaking at ridge tops
Recent example - Haiti (Susan Hough)

Hotel Montana
(at the top of a ridge)

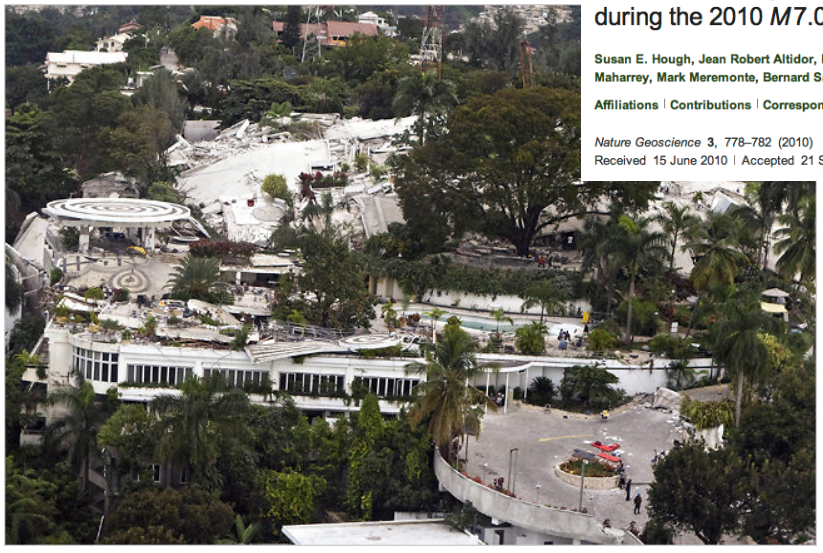

nature geoscience

nature.com ▸ journal home ▸ archive ▸ issue ▸ letter ▸ abstract

NATURE GEOSCIENCE | LETTER

Localized damage caused by topographic amplification during the 2010 *M*7.0 Haiti earthquake

Susan E. Hough, Jean Robert Altidor, Dieuseul Anglade, Doug Given, M. Guillard Janvier, J. Zebulon Maharrey, Mark Meremonte, Bernard Saint-Louis Mildor, Claude Prepetit & Alan Yong

Affiliations | Contributions | Corresponding author

Nature Geoscience **3**, 778–782 (2010) | doi:10.1038/ngeo988
Received 15 June 2010 | Accepted 21 September 2010 | Published online 17 October 2010

Topographic Effects

$$\lambda = \frac{V}{f} \approx \frac{2000\ m\ s^{-1}}{10\ Hz} \approx 200\ m$$

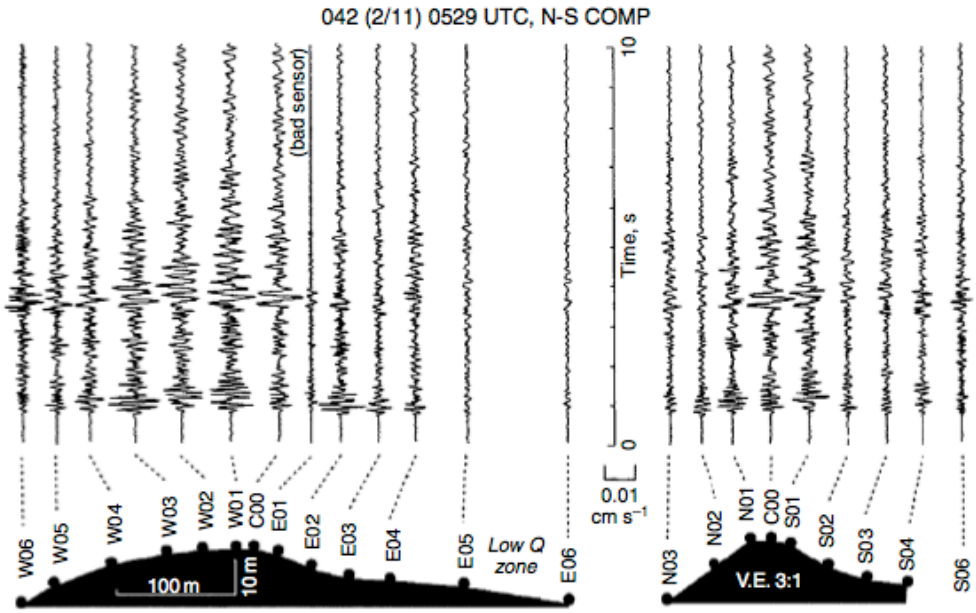

Figure 15 North-south component of seismograms from an aftershock of the 1994 Northridge earthquake, recorded at several stations on a 20-m-high topographic feature south of the earthquake. The seismograms on the left show a profile along the long, east–west axis of the hill, and the seismograms on the right show a north–south profile transverse to the hill. Note how the records show higher amplitudes on the hill than at stations at the base of the hill. From Spudich PA, Hellwig M, and Lee WHK (1996) Directional topographic response at Tarzana observed in aftershocks of the 1994 Northridge, California, earthquake: Implications for mainshock motions. *Bulletin of the Seismological Society of America* 86(1B): S193–S208.

Theoretical Models for estimation of strong shaking

Stochastic: band-limited white noise in frequency domain

One important approach to generating synthetic seismograms was proposed by Boore (1983). In this approach, one generates a completely random time series, applies a shape function in the time domain so that the time series has a reasonable envelope of amplitude with time, transforms to the frequency domain, modifies the Fourier amplitude spectrum to match the amplitude and shape of a spectral model, and then transforms back to the time domain to obtain the synthetic seismogram. The representation theorem is thus applied in the frequency domain

Synthetic Greens Functions:

Derived from full space solution, enforcing traction-free surface
Generally available for 1-D (layered) elastic structure (with all terms)
JF's term project

Empirical Greens Functions:

Greens functions are seissmic records of small earthquakes
Assume focal mechanism is same as for larger future quake
Records are not always available for desired source-receiver pairs

954-957

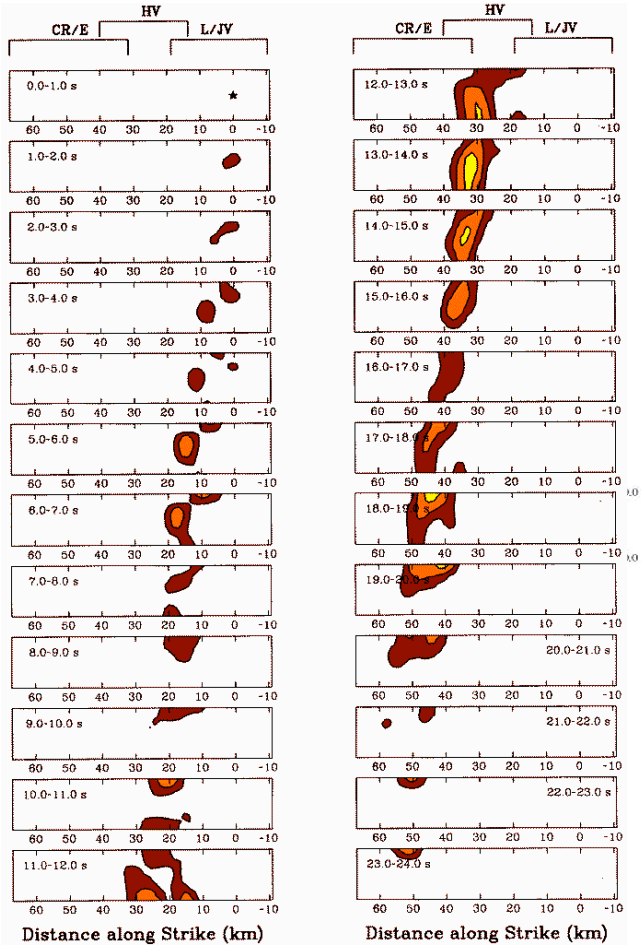

To model strong motion:
at each snapshot, you need
slip and slip rate on each discrete
patch of the fault

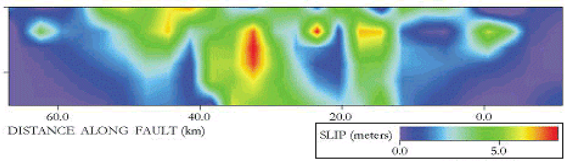

Wald and Heaton, 1994

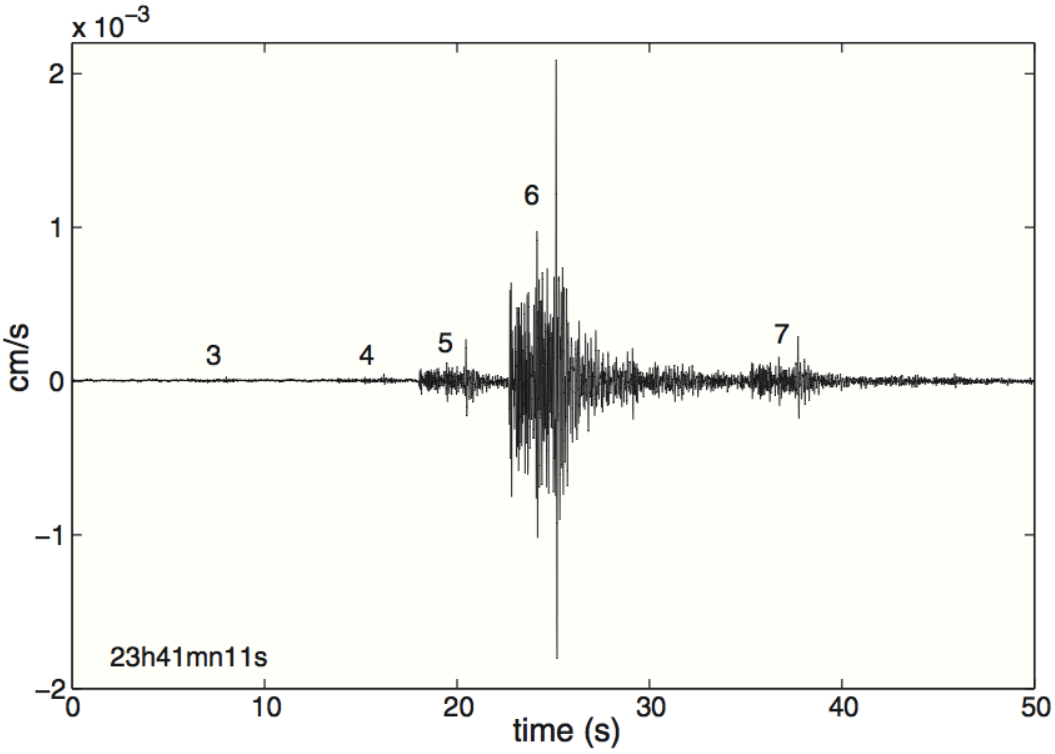

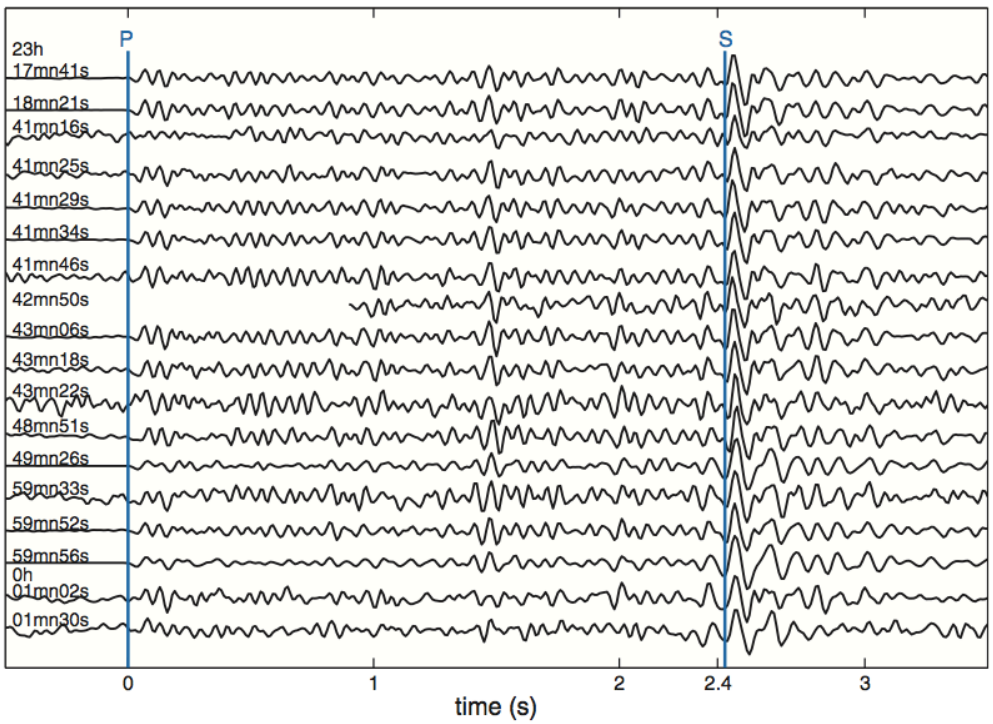

Fig. 2. Records of the foreshocks, arranged in chronological order from top to bottom. The starting time of each trace, the *P*-wave arrival, and the *S*-wave are indicated. Each trace is normalized to its peak amplitude, given in table S1. The origin of the time axis corresponds to the *P*-wave arrival.

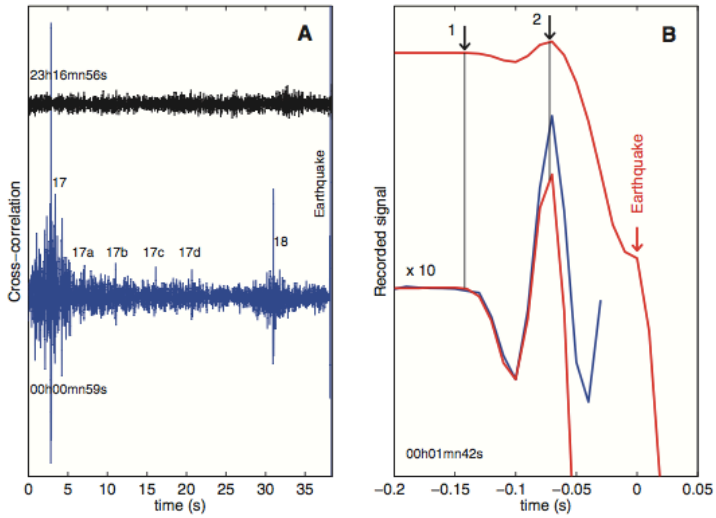

Fig. 3. (**A**) Signals obtained by cross-correlating the waveform of one of the foreshocks with the records. The top trace corresponds to the beginning of the first triggered window and occurs before the first foreshock. The bottom trace corresponds to the ground motion in the 40 s preceding the earthquake. Peaks in the correlation show the occurrence of several events with waveforms similar to the template. Numbers 17 and 18 refer to the chronological order of the foreshocks in Fig. 2. Peaks 17, a to d, are interpreted as four newly detected events. (**B**) Seismic signal immediately preceding the earthquake. The recorded ground motion (top trace) shows the occurrence of two shocks 0.14 and 0.07s before the earthquake. The lower red trace shows the first part of the same record amplified 10 times compared with the *P* waveform of the prior foreshocks (shown in blue, foreshock 2).

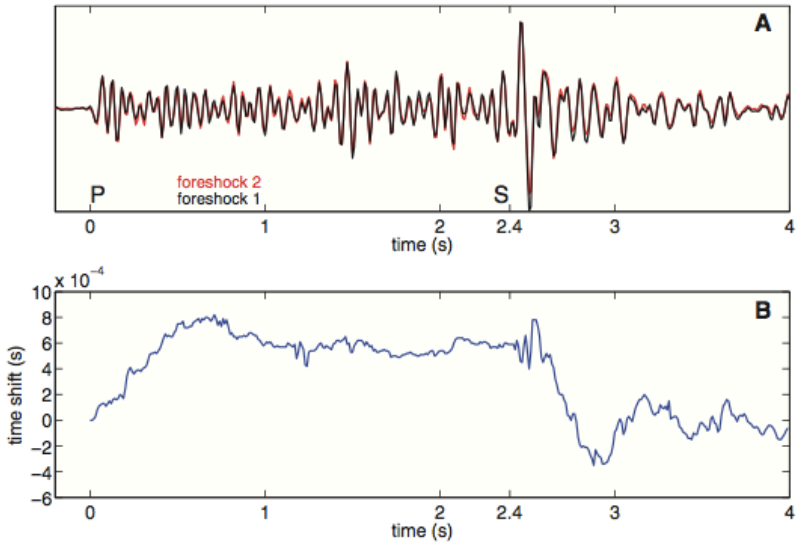

Fig. 4. (**A**) Superposition of the records of the first and second foreshocks. The second record has been shifted in time (in the Fourier domain) by the time increment that maximizes the cross-correlation of the two signals. The beginnings of the *P* and *S* waves are indicated. The *P* arrivals correspond to the origin of the time axis. The nonzero amplitude before the *P* arrivals shows the noise level of the records. (**B**) Evolution of the time shift that maximizes the correlation between the waveforms of the first two foreshocks. The correlation is done over a moving window 128 points long (1.28 s). The first window begins at the *P*-wave arrival and corresponds to the origin of the time axis. Subsequent time shifts are measured relative to this first window. The time shift is obtained by interpolating the correlation peak at each time step.

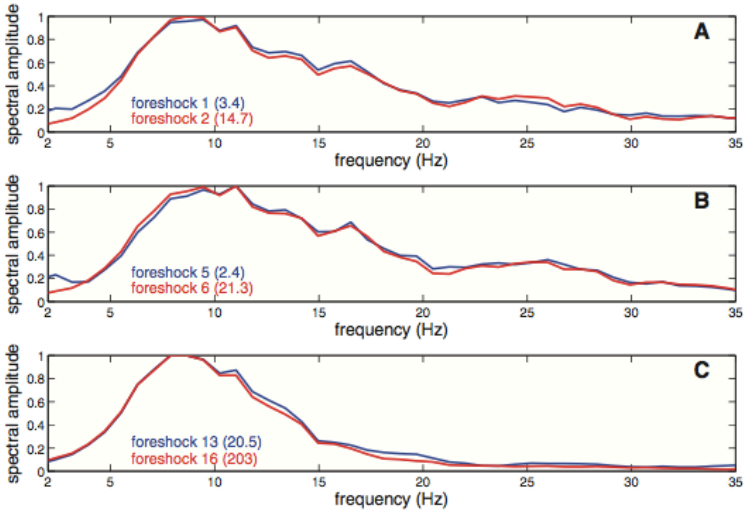

Fig. 5. (**A** to **C**) Comparison of the *S*-wave ground-velocity spectra of some events. Numbers refer to the chronological order of the foreshocks in Fig. 2. All of the spectra are corrected for the instrument response and normalized independently. Spectral amplitudes below 5 Hz are affected by the low-frequency background seismic noise, which scales differently from event to event. The peak recorded amplitude of each event is given in parenthesis and is expressed in micrometers per second. The two largest shocks are shown in (**C**).

Fig. 6. Ground motion recorded in the first triggered window (bottom trace) and corresponding signal low-pass filtered below 3 Hz (top trace). Numbers indicate the first two foreshocks.

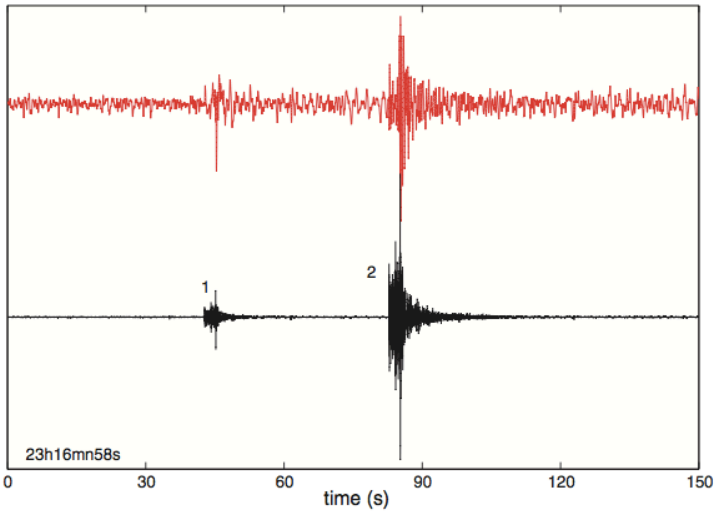

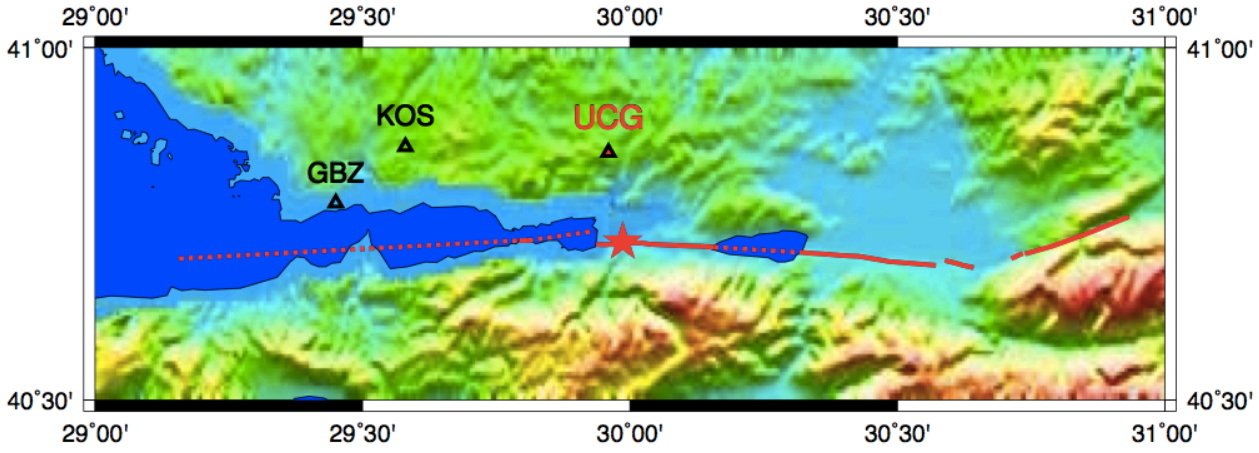

Figure S1

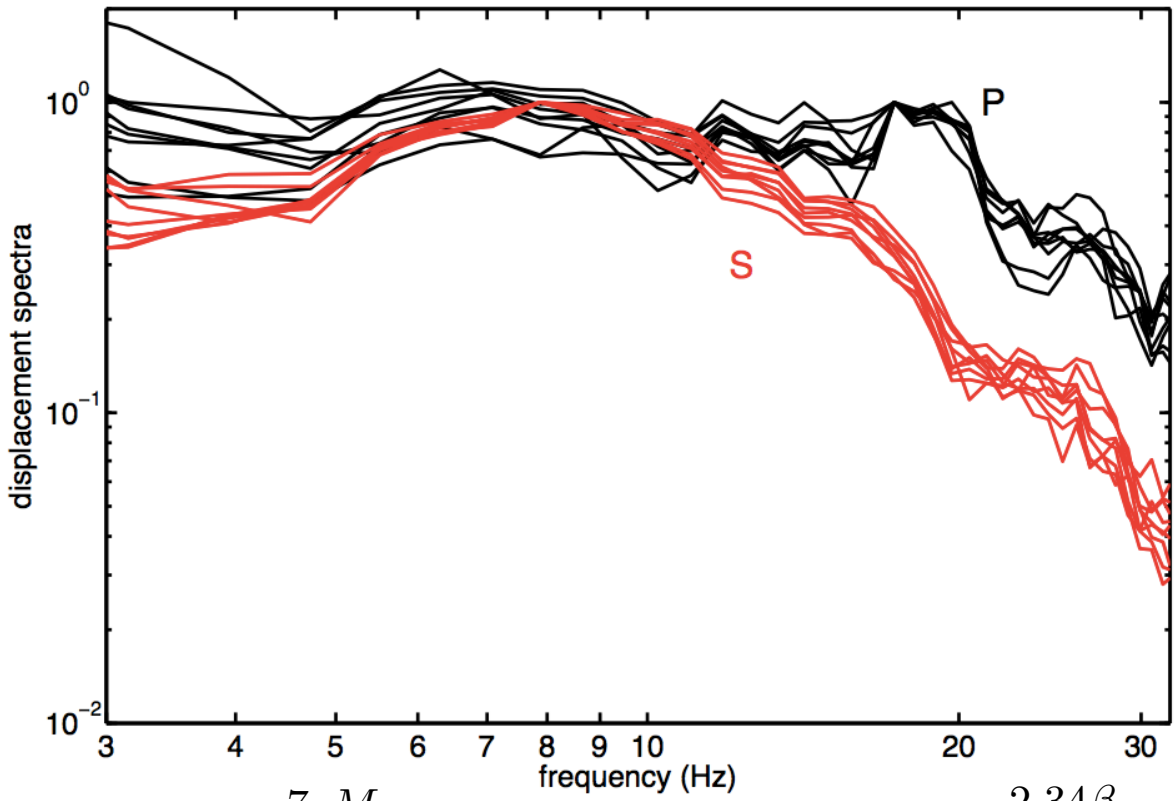

$$\Delta\sigma = \frac{7}{16}\frac{M_o}{r^3}$$

Figure S2

$$r = \frac{2.34\beta}{2\pi f_c}$$

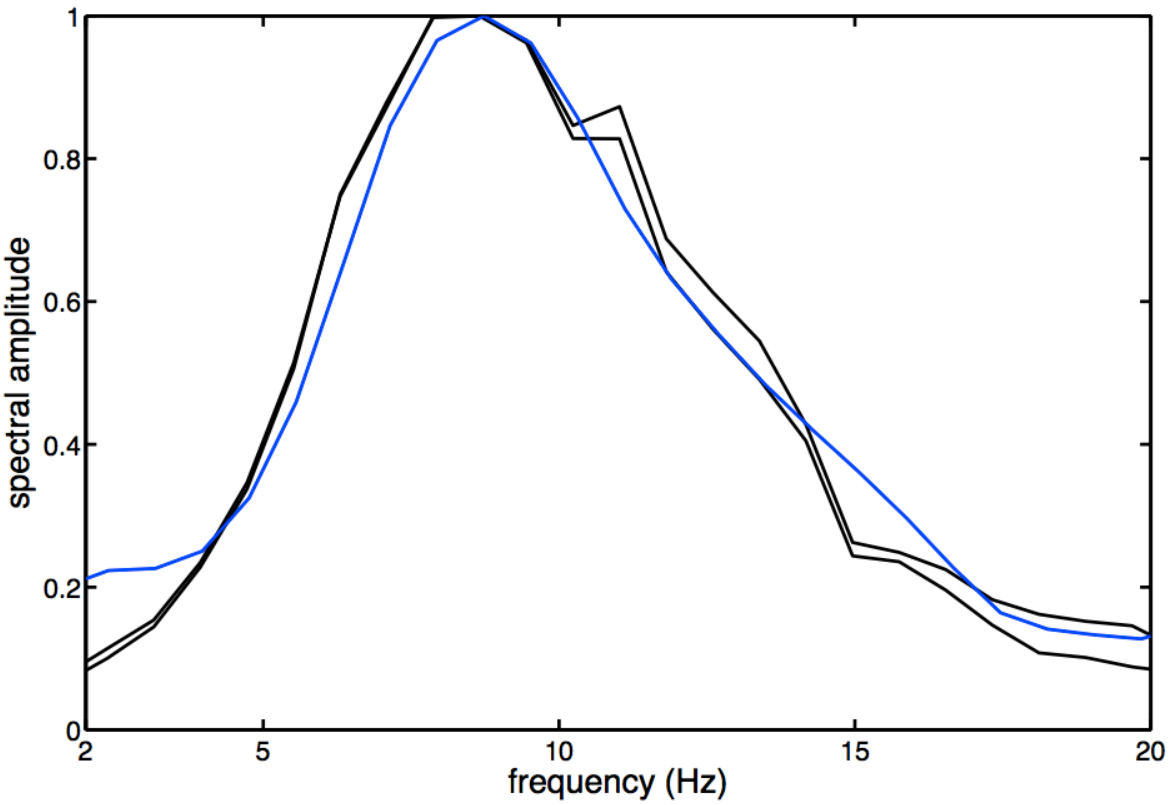

Figure S3

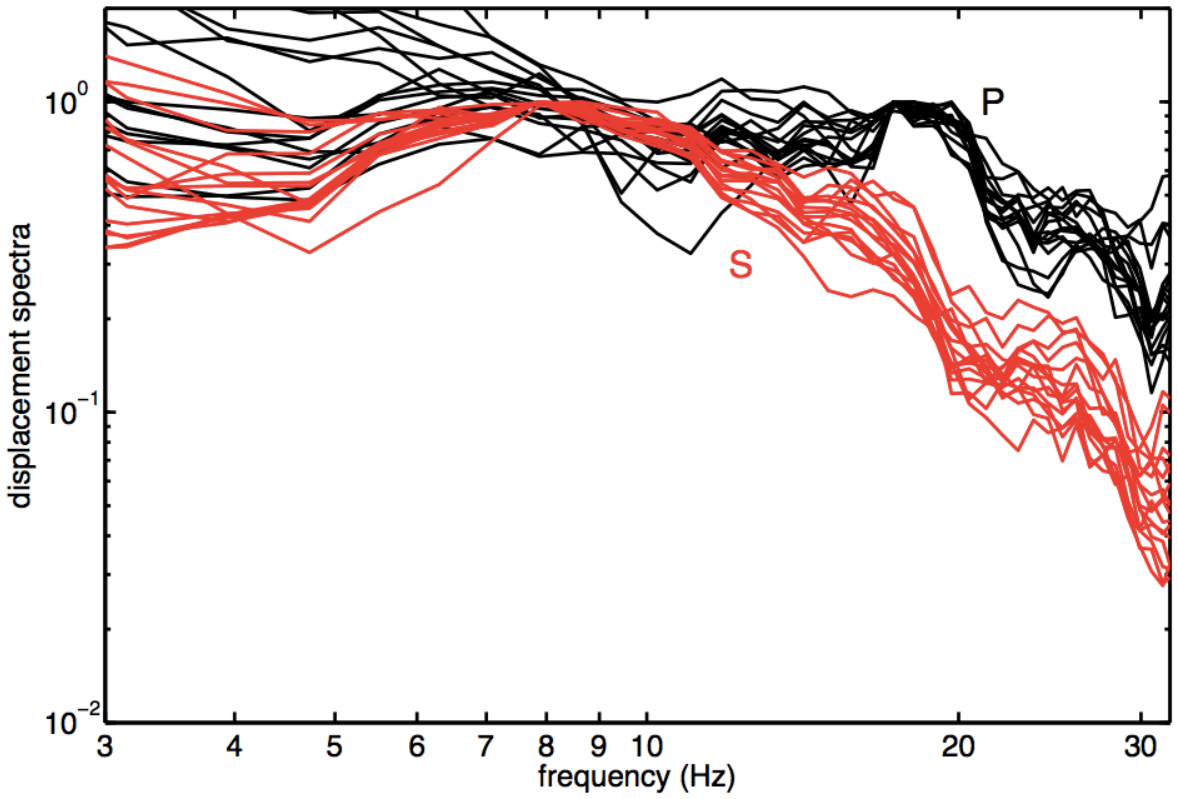

Figure S4

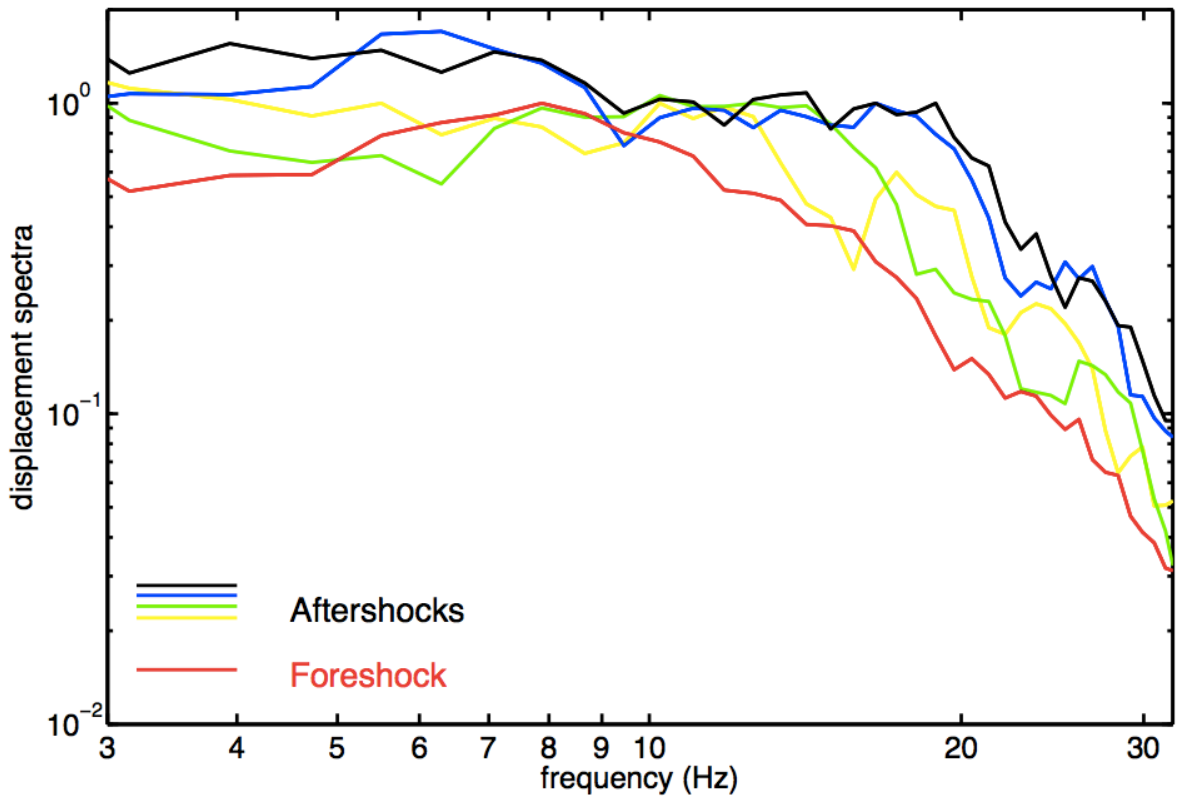

Figure S5

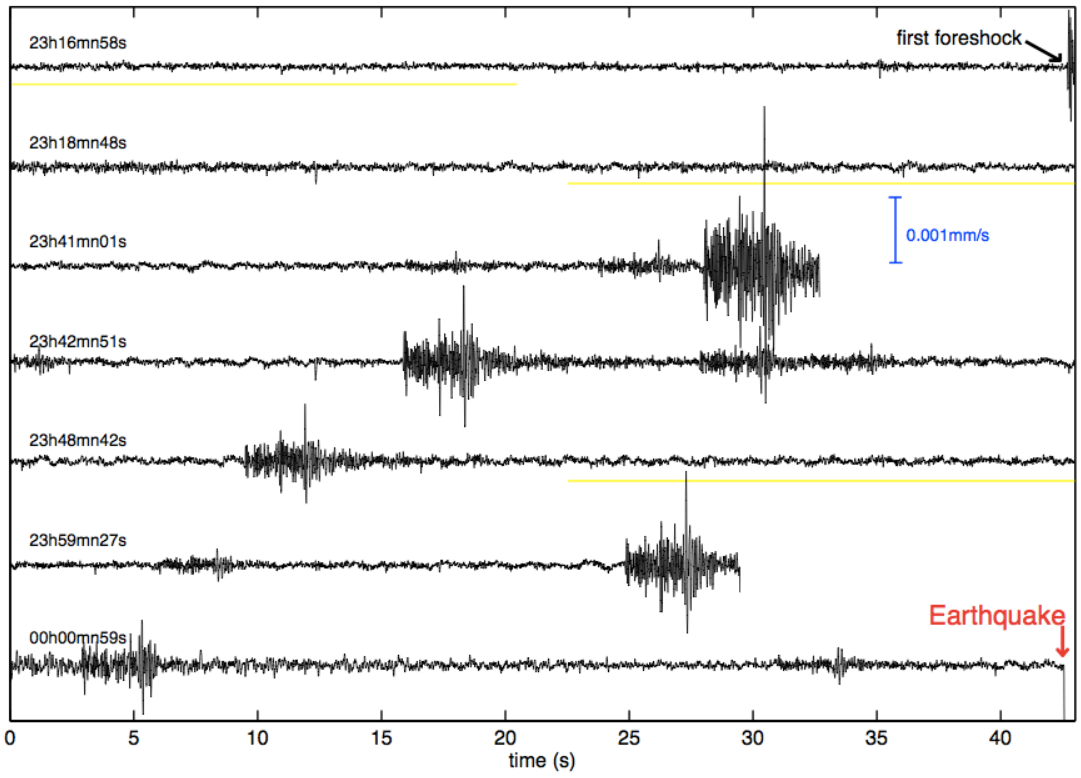

Figure S6

k relates slip (offset) to the shear stress change

Equation for stiffness k for a small, elliptical crack is:

$$k = \frac{G}{(1-\nu)L}$$

G = shear modulus
ν = Poisson's ratio
L = length of slipping area

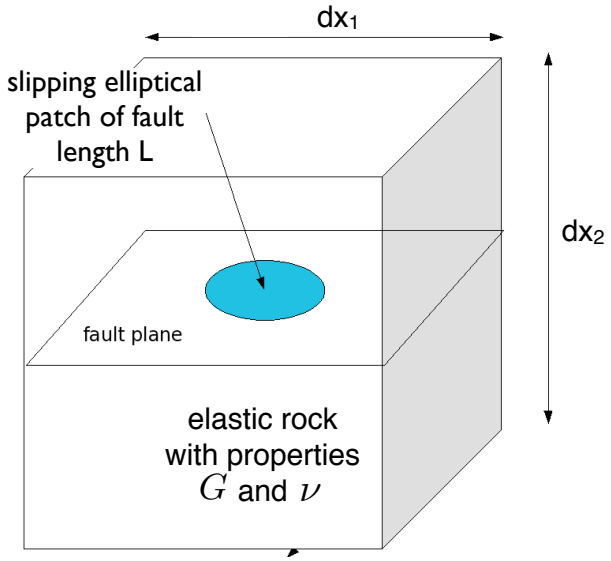

Earthquake machine: k is the spring stiffness

Earth: k is the elastic force due to offset along crack (length L)

$$k < \frac{\sigma_n (b-a)}{D_c}$$

$$\frac{G}{(1-\nu)L} < \frac{\sigma_n (b-a)}{D_c}$$

k = crack stiffness
G = shear modulus
ν = Poisson's ratio
L = length of slipping area
$(b-a)$ = friction weakening parameter
σ_n = normal stress
D_c = friction weakening distance

$$L > \frac{D_c G}{(1-\nu)(b-a)\sigma_n}$$

This tells us that the slipping patch of fault must be bigger than a critical size to go unstable, *even* for a velocity weakening fault

$$L > \frac{D_c G}{(1-\nu)(b-a)\sigma_n}$$

This tells us that the slipping patch of fault must be bigger than a critical size to go unstable, *even* for a velocity weakening fault

Typical values in the seismogenic zone:

Dc = 10 microns (based on experiments)
larger?? (based on minimum measured earthquake size)
G = 30 GPa
(b-a) = around 10^{-2}
eff normal stress = 2e8 Pa at 10 km depth
L > 0.15 m at 10 km, 1.5 m at 1 km.
in mines: 15 m patch of slip measured (M 0) in mine at 1 km depth

This implies a finite nucleation time.

http://www.sciencenetlinks.com/sci_update.php?DocID=216

Nucleation time: shallow crust: of the order of a month to a year?

12 hours is too short (no correlation with Earth tides)

tremor and volcanic quakes are triggered by passing surface waves - so nucleation times must be very fast.

on the Moon - nucleation is very fast (is it even friction?)

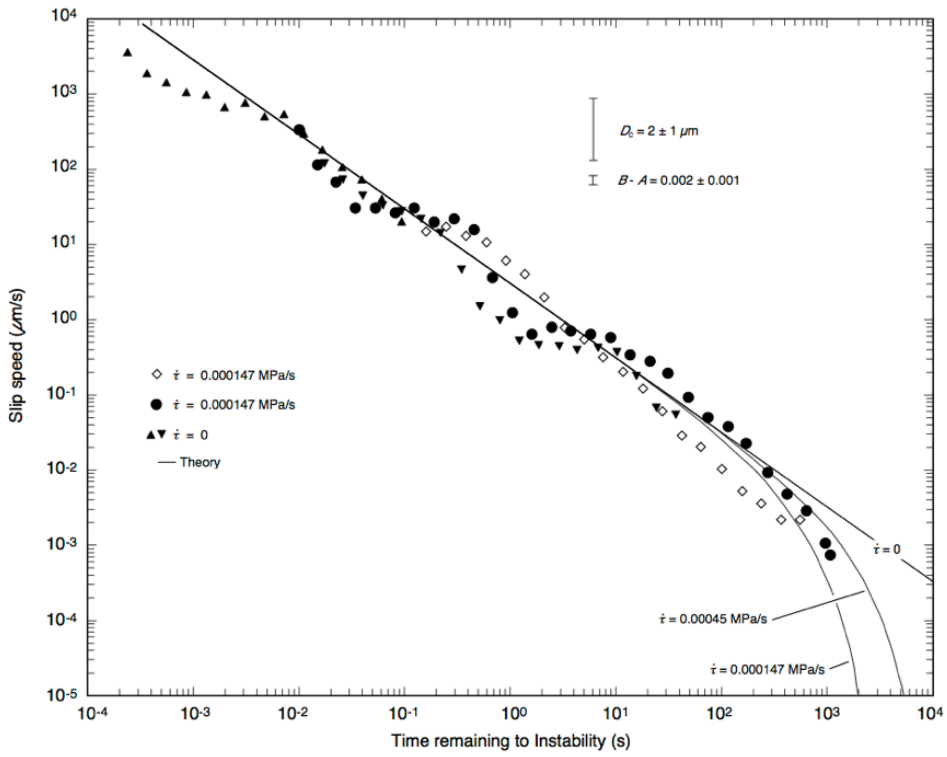

FIG. 5. Comparison of theory and laboratory observations of the time remaining to instability and speed of premonitory slip. Experimental data were obtained at the indicated stressing rates using the large biaxial apparatus employed for the experiment of Fig. 3. The curves give the solutions of Eqs. **10** and **11** at the stressing conditions of the experiments. The error bars indicate the sensitivity of the solutions to the uncertainties in constitutive the parameters D_c and $(B - A)$.

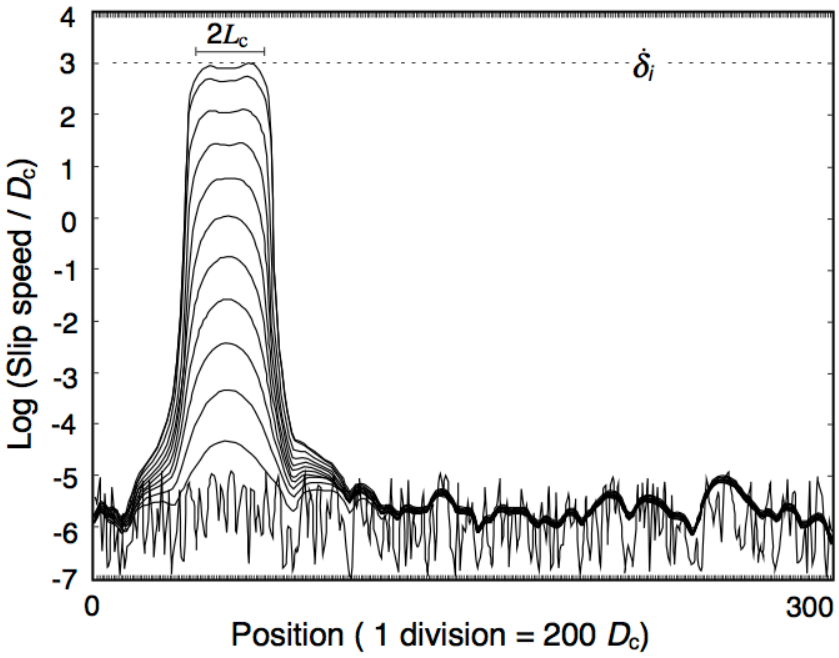

FIG. 4. Numerical model of accelerating slip leading to instability on a fault with 300 fault elements and randomized initial shear stress from Dieterich (24) showing slip speeds at successive times in the calculation. The interval between time steps decreases as slip speed increases. Every 50th step is shown. $\dot{\delta}_i$ is the assumed slip speed at initiation of unstable slip. L_c is the characteristic length from Eq. **9**.

Asperity is being loaded by creep on adjoining parts of fault that are assumed to be velocity-weakening (unstable) but not creeping over a large enough area to go unstable (creep rate accelerates with time as theory predicts)

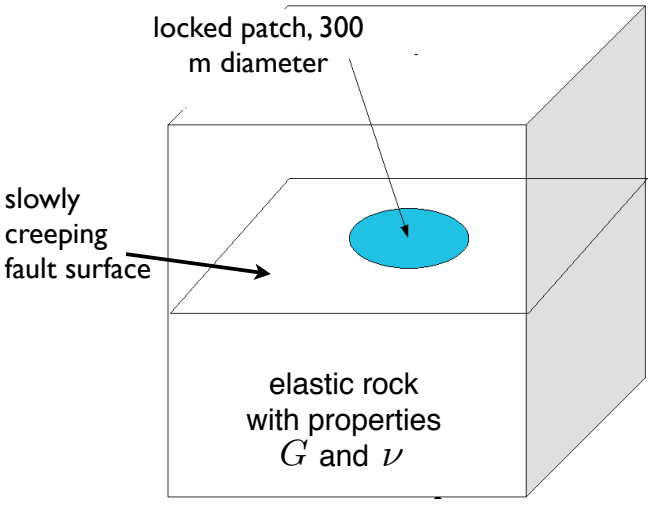

$$L > \frac{D_c G}{(1-\nu)(b-a)\sigma_n}$$

Asperity L is small

locally low normal stress due to high pore pressure?

locally large (b-a)?

patch surrounded by velocity-strengthening material?

Slow earthquakes

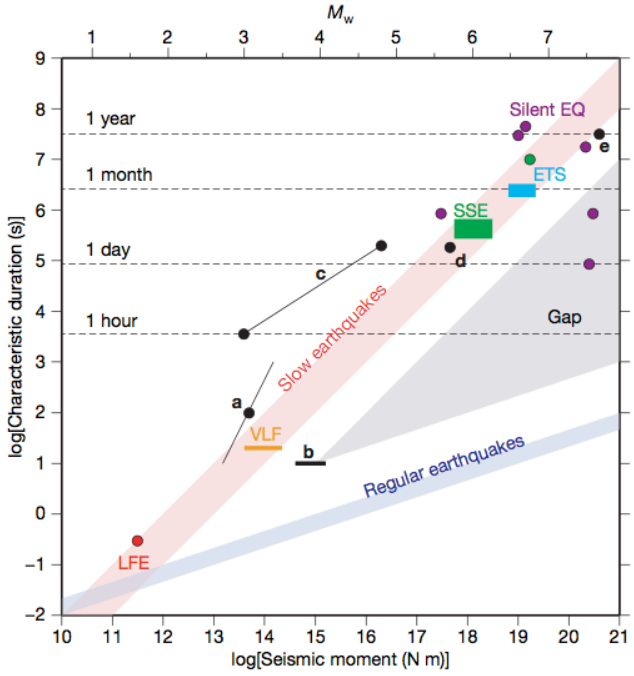

Ide et al., 2007

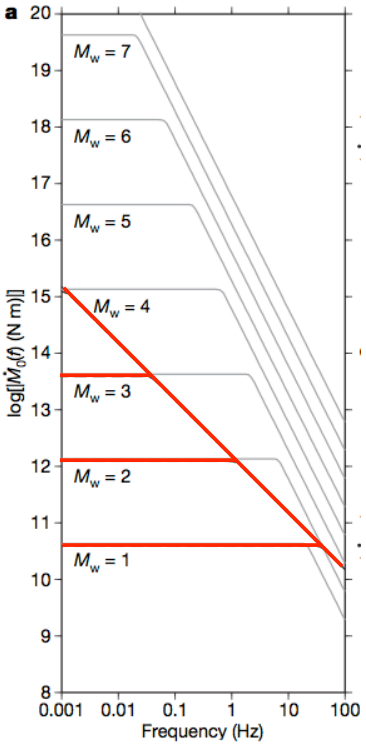

Ide et al., 2007

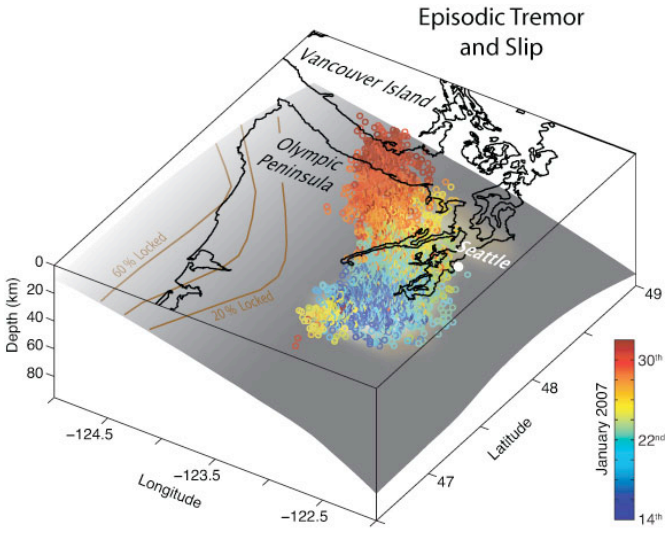

K. Creager, University of Washington.

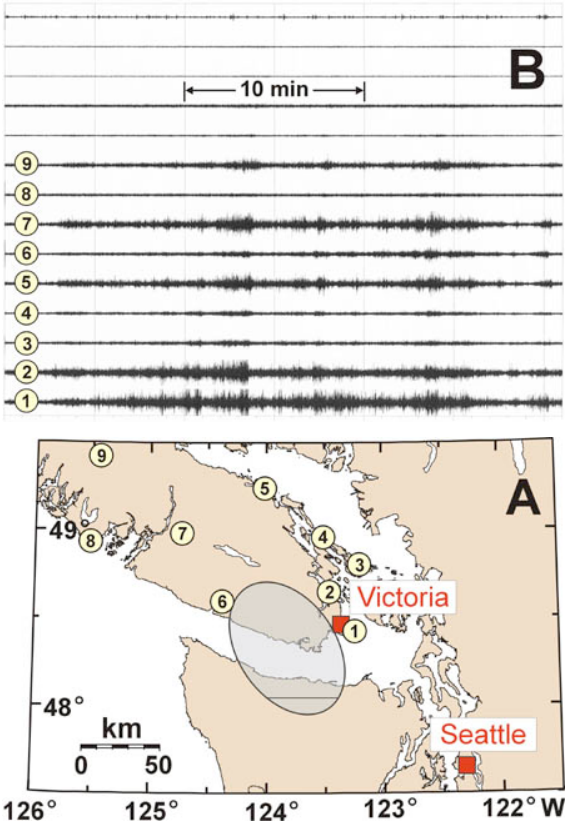

http://earthquakescanada.nrcan.gc.ca/pprs-pprp/re/ETS-eng.php